Supplementary Material to Longstaff et al. "Neutralisation of the anti-coagulant effects of heparin by histones in blood plasma and purified systems" (Thromb Haemost 2016; 115.3)

Surface plasmon resonance (SPR)

SPR work was performed at 25 ˚C using a Biacore T100 machine incorporating a CM4 sensor chip (GE Healthcare, Uppsala, Sweden). Standard amine coupling was employed to immobilise histones (Sigma, type IIIS), and binding studies were performed at a flow rate of 5 µl/min in 10 mM HEPES 150 mM NaCl pH 7.4 containing 0.01% surfactant P20. Specific binding expressed as binding stability (RU) was measured by subtracting nonspecific binding to a histone-free control surface using the in-line reference subtraction feature of the instrument. Data are summarised in Figure S1 for the binding of UFH, LMWH IS and Enoxaparin to immobilised histone, with and without competition with 50 µg/ml DNA pre-mixed with a range of heparin concentrations.

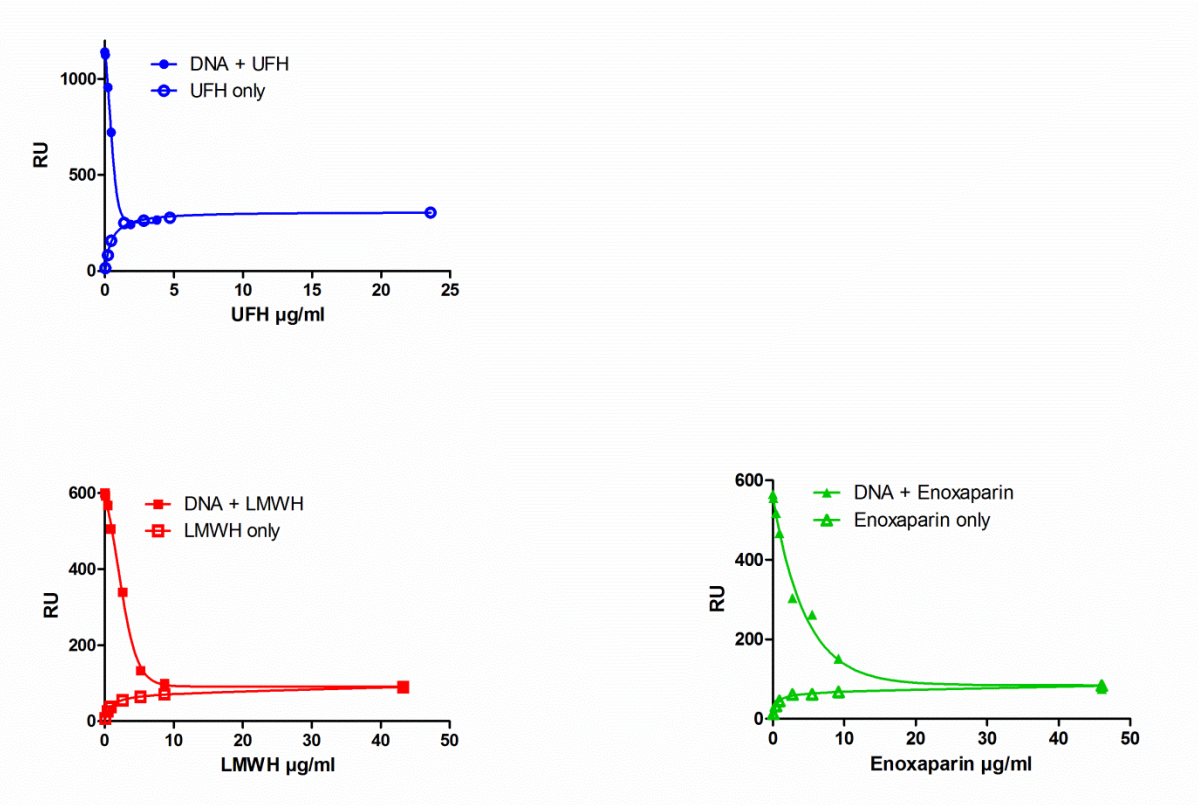

Suppl. Figure 1: Binding of heparins and DNA to immobilised histones studied by SPR. Binding of heparins to immobilised histones is indicated by open symbols and curves are fitted to a single site binding isotherm to calculate apparent equilibrium dissociation constants. Competition with added 50 µg/mL DNA is indicated by the solid symbols and data were fitted to a four parameter, log [inhibitor] versus response model (GraphPad Prism), to yield estimates for apparent IC_{50} values for the inhibition by heparins of binding of DNA to histones.

Permeability studies

Porosity of fibrin network was assessed from the liquid permeability of the clots under constant hydrostatic pressure. Fibrin clots were formed in disposable plastic pipette tips using 15 nM thrombin and a 2.5 g/l fibrinogen solution in 10 mM Hepes 150 mM NaCl pH 7.4 containing UFH or LMWH at 0.25 IU/ml anti IIa concentration. Clotting was allowed to proceed for 70 min at 37 °C, thereafter buffer was loaded on top of the clots and fluid passing through the clots was measured in a collecting tube attached to the bottom of the clot. The permeability coefficient was calculated according to the equation $K_S = \frac{Q.L.\eta}{t.A.\Delta P}$, where Q = permeated volume of buffer (cm^3); η = viscosity of buffer; L = clot length; A = average cross-sectional area of the clot; t = time (s); ΔP = pressure drop. Permeability constants are presented in relative units, considering pure fibrin permeability as 1. Since we did not observe a significant concentration dependency in the studied heparin concentration range, we present data at the lowest heparin concentrations, which match the concentration range used in the other methods, as well.

Scanning electron microscope (SEM) imaging of fibrin

Following 30 min clotting of 2.5 mg/ml fibrinogen containing different additives indicated for each measurement with 5 nM thrombin, fibrin clots of 100-µl volume were placed into 10 ml 100 mM Na-cacodylate pH 7.2 buffer for 24 h at 4 °C. Following repeated washes with the same buffer, samples were fixed in 1 %(v/v) glutaraldehyde for 16 h. The fixed samples were dehydrated in a series of ethanol dilutions (20 – 96 %(v/v)), 1:1 mixture of 96 %(v/v) ethanol/acetone and pure acetone followed by critical point drying with CO_2 in E3000 Critical Point Drying Apparatus (Quorum Technologies, Newhaven, UK). The specimens were mounted on adhesive carbon discs, sputter coated with gold in SC7620 Sputter Coater (Quorum Technologies, Newhaven, UK) and images were taken with scanning electron microscope EVO40 (Carl Zeiss GmbH, Oberkochen, Germany).

Structural characterization of fibrin by small-angle X-ray scattering (SAXS)

Fibrin samples with the same composition as those used for the SEM evaluation (2.5 mg/ml fibrinogen, 5 nM thrombin) and 25 µg/ml UFH or LMWH were examined by SAXS measurements performed on the four-crystal monochromator beamline[1] of Physikalisch-Technische Bundesanstalt (PTB, Berlin, Germany) supplemented by the SAXS setup[2] of Helmholtz-Zentrum Berlin at the synchrotron radiation facility BESSY II (HZB, Berlin, Germany). The samples were filled into glass capillaries with 1.0 mm diameter. The energy of the incoming X-ray beam was 8 keV and the 2D scattering patterns were collected with a vacuum-compatible large-area pixel detector Pilatus 1M (Dectris Ltd., Baden, Switzerland). Measurements were performed at sample-to-detector distance of 1.5 meter, which covers the range of momentum transfer of q = 0.1 nm^{-1} to 2 nm^{-1} ($q = 4\pi/\lambda \sin\theta$, where θ is half the scattering angle and λ is the wavelength of the incident X-ray beam). All measurements were carried out at room temperature. The scattering curves were obtained by radial averaging of the 2D patterns.[3] For quantitative analysis of the scattering pattern, non-linear least-square fitting of an empirical model function to the scattering curves was performed using the SASfit program v. 0.93.5 (Joachim Kohlbrecher and Ingo Bressler, Paul Scherrer Institute, Villigen,

Switzerland), in which the peaks were approximated by Lorentzian functions, whereas the decay trend was taken into account by a power-law function.

Results

The general decay trend of the scattering curves (Fig. SAXS) reflects the fractal structure of the fibrin clot and its effect can be modelled as a background signal with empirical power-law functions in the form of $C_0+C_4*q^{-\alpha}$ (Suppl. table S1). The peaks arising above this background reflect the longitudinal and cross-sectional alignment of fibrin monomers. A small, but sharp peak in pure fibrin at *q*-value of ~0.290 nm^{-1} (Suppl. Figure S2, Peak (2) in Suppl. table S1) corresponds to the longitudinal periodicity of $d = 2\pi/q' = 22$ nm that is in agreement with earlier SAXS studies and is not resolvable in the case of UFH and its center was slightly shifted to 0.303 nm^{-1} by LMWH. The most pronounced effect of UFH and LMWH was observed on the broad scattering peak spanning over the *q*-range of ~0.2 to 0.5 nm^{-1} corresponding to the cluster units of the fibers (Fig. S2, Peak (1) in Suppl. table S2). The central position of this peak was shifted from 0.284 nm^{-1} to 0.331 nm^{-1} by UFH and to 0.383 nm^{-1} by LMWH, which corresponds to a reduction in the periodicity distance from 22.1 nm to 19.0 nm and 16.4 nm, respectively, in line with the decrease in fiber size observed with SEM (Table). The second broad peak (from ~0.6 to 1.2 nm^{-1}, Peak (3) in Suppl. table S2) is slightly shifted to a lower *q*-range by UFH and LMWH, suggesting a mild increase in the average protofibril-to-protofibril distance according to the structural models of Yang et al. and Weisel (4,5). However, the overall structural alteration of fibrin is dominated by the tighter packing in the cluster units of the fibers resulting in a network of thinner fibers and smaller pores as evidenced by the SEM and permeability data (Table 1).

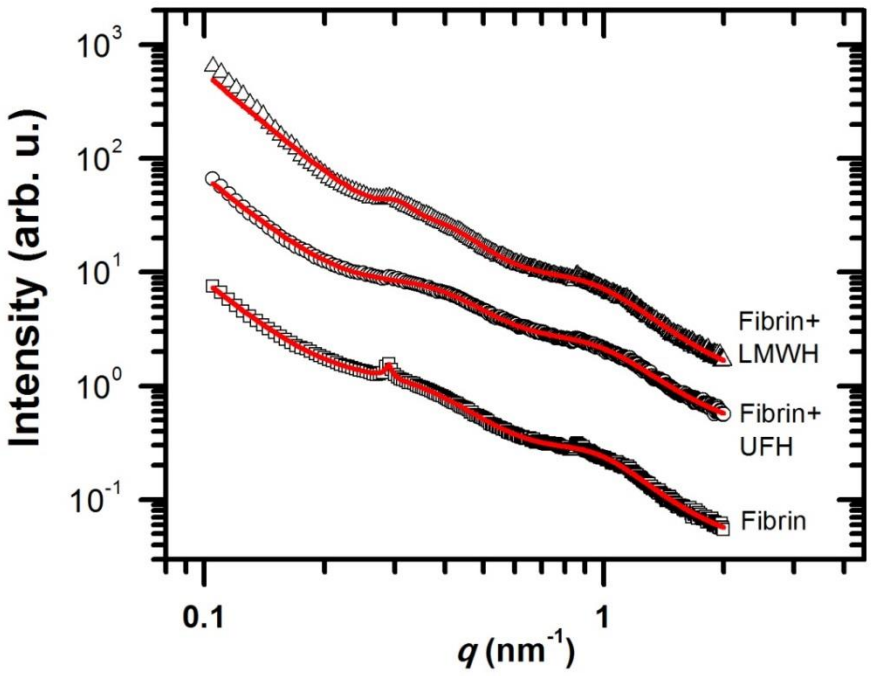

Suppl. Figure 2.

Suppl. Table 1: Parameters of the empirical functions used to interpret the SAXS data.

Contribution	Parameter	Fibrin	Fibrin+UFH	Fibrin+LMWH
Background (1)	C_0	0.029±0.0007	0.029±0.0009	0.024±0.0004
	C_4	0.0087±0.0006	0.019±0.0001	0.00063±6.4 x 10^{-5}
	α	2.96±0.03	2.96±0.000	3.00±0.000
Peak (1)	Area	0.457±0.012	0.303±0.005	0.179±0.012
	Center / nm^{-1}	0.284±0.002	0.331±0.001	0.383±0.005
	Width / nm^{-1}	0.188±0.002	0.187±0.002	0.136±0.004
Peak (2)	Area	0.068±0.0003	n/a	0.040±0.006
	Center / nm^{-1}	0.290±0.002	n/a	0.303±0.0009
	Width / nm^{-1}	0.0058±0.0003	n/a	0.037±0.003
Peak (3)	Area	0.198±0.004	0.218±0.006	0.288±0.008
	Center / nm^{-1}	0.887±0.004	0.858±0.005	0.823±0.006
	Width / nm^{-1}	0.385±0.005	0.453±0.007	0.451±0.006

The background SAXS data at low q values (Fig. SAXS) was approximated by a power law decay with a constant background ($C_0+C_4*q^{-\alpha}$). The three peak functions centered around 0.28 to 0.38 nm^{-1} (Peak 1), 0.29 nm^{-1} (Peak 2) or 0.82 to 0.89 nm^{-1} (Peak 3), were approximated by Lorentzian functions. The physical interpretation of the $C_0+C_4*q^{-\alpha}$ formula is based on the fractal structure of the fibrin clot as applied in our earlier report (6)

Suppl. References

1. Krumrey M, Ulm G. High-accuracy detector calibration at the PTB four-crystal monochromator beamline. Nucl Instrum Methods Phys Res Sect Accel Spectrometers Detect Assoc Equip. 2001; 467: 1175-1178.

2. Gleber G, Cibik L, Haas S, et al.. Traceable size determination of PMMA nanoparticles based on Small Angle X-ray Scattering (SAXS). J Phys Conf Ser. 2010; 247: 012027.

3. Krumrey M, Gleber G, Scholze F, et al. Synchrotron radiation-based x-ray reflection and scattering techniques for dimensional nanometrology. Meas Sci Technol. 2011; 22(9): 094032.

4. Weisel JW. The electron microscope band pattern of human fibrin: various stains, lateral order, and carbohydrate localization. J Ultrastruct Mol Struct Res. 1986; 96(1-3): 176-188

5. Yang Z, Mochalkin I, Doolittle RF. A model of fibrin formation based on crystal structures of fibrinogen and fibrin fragments complexed with synthetic peptides. Proc Natl Acad Sci U S A. 2000; 97(26): 14156-14161

6. Longstaff C, Varju I, Sotonyi P, et al. Mechanical stability and fibrinolytic resistance of clots containing fibrin, DNA, and histones. J Biol Chem 2013; 288(10): 6946-6956.